Crystal structure and physical properties of UAuSi and UAu_2

Rainer Pöttgen,[a] Vinh Hung Tran,[b] Rolf-Dieter Hoffmann,[a] Dariusz Kaczorowski[b] and Robert Troc[b]
[a]*Anorganisch-Chemisches Institut, Universität Münster, Wilhelm-Klemm-Strasse 8, D-48149 Münster, Germany*
[b]*W. Trzebiatowski Institute for Low Temperature and Structure Research, Polish Academy of Sciences, PO Box 937, 50–950 Wrocław, Poland*

UAuSi and UAu_2 have been prepared by arc-melting of the elemental components and subsequent annealing. The crystal structure of UAuSi, which has been previously reported to crystallize in the TiNiSi-type structure, was determined from X-ray powder diffraction data: LiBaSi-type structure, $P\bar{6}m2$, $a=419.5(2)$ pm, $c=397.2(2)$ pm, $V=0.0605$ nm^3, $Z=1$ and $R_B(I)=0.018$. It is derived from the AlB_2-type structure by an ordered arrangement of the gold and silicon atoms on the boron sites. The binary compound UAu_2 (AlB_2-type) is confirmed. Magnetic susceptibility measurements indicate spin-glass behaviour and paramagnetism for UAuSi and UAu_2, respectively. Both compounds are metallic conductors.

The binary uranium silicide β-USi_2 adopts the hexagonal structure of AlB_2.[1,2] The same structure was also reported for UAu_2.[3,4] However, Dommann and Hulliger[5] reported UAu_2 with the $CeCd_2$-type structure,[5] which is derived from that of AlB_2 by simply shifting the gold position from $z=0.5$ to $z=0.45$, resulting in slightly puckered layers.

Thus, the silicon atoms in β-USi_2 should be substitutable by gold atoms. We recently reported on U_2AuSi_3,[6] the first compound in the pseudo-binary system USi_2–UAu_2. Similar U_2TSi_3 compounds exist with other transition metals.[7–9] Another compound in this system is UAuSi,[10] previously reported to adopt the orthorhombic structure of TiNiSi; susceptibility measurements on this compound indicated spin-glass behaviour. We have reinvestigated the crystal structure of UAuSi and observed some inconsistencies with the previous data. Herein we show that UAuSi adopts the hexagonal structure of LiBaSi, an ordered derivative of the AlB_2-type structure. In addition we report in detail on the physical properties of UAuSi and UAu_2.

Experimental

Starting materials were uranium platelets (Merck, 'nuklearrein'), gold wire (Degussa, >99.9%) and silicon lumps (Merck, >99.9%). The uranium platelets were cleaned with concentrated nitric acid to remove oxide impurities and were then kept under argon. The samples were prepared by arc-melting the elements in an argon atmosphere. The argon was purified by repeatedly melting titanium sponge prior to the reactions. The molten buttons were turned over and remelted three times on each side to ensure homogeneity. The mass losses after several meltings were always <0.5%. The samples were subsequently wrapped in tantalum foil and annealed in evacuated sealed silica tubes at temperatures between 650 and 800 °C for 2 weeks.

Guinier powder patterns of all samples were recorded with Cu-Kα_1 radiation and α-quartz ($a=491.30$ pm, $c=540.46$ pm) as internal standard. Air-sensitive UAu_2 was ground to powder with dried paraffin oil and placed between two scotch tapes to prevent hydrolysis. The lattice parameters (Table 1) were obtained by least-squares refinements. The indexing was facilitated by intensity calculations.[11]

Powder diffraction measurements of the UAuSi samples were performed on a STOE STADI/P focusing monochromatic beam diffractometer with a rotating very flat sample in the symmetric transmission mode. Cu-Kα_1 radiation was used with a linear position-sensitive detector, a step width of 0.02° (2θ) and a counting time of 20 s per step. The Rietveld refinements were performed with the RIETAN program.[12]

The magnetic susceptibilities of polycrystalline samples were measured in the temperature range 4.2–300 K using an RH-Cahn electrobalance.

Electrical resistivity measurements were performed in the temperature range 4.2–300 K with a conventional four-point technique. The sample voltage was measured automatically every 20 s with an accuracy of ± 1 μV. The measurements were repeated with different samples, and the results were reproducible.

Results and Discussion

Crushed buttons of the samples are all light grey with a metallic lustre; powders are dark grey. The silicon-rich samples up to composition UAuSi are stable in air over several months; however, UAu_2 was less stable and showed some hydrolysis. These samples were kept under vacuum. The sensitivity against traces of humidity of such gold compounds was also observed for the corresponding thorium compound[13] as well as for the alkali-metal gold compounds KAu_5,[14] $NaAu_2$,[15] RbAu[16] and Rb_2Au_3.[17]

Table 1 Lattice parameters of the hexagonal binary and ternary compounds in the pseudo-binary system USi_2-UAu_2[a]

compound	structure type	a/pm	c/pm	c/a	V/nm^3	ref.
β-USi_2	AlB_2	402.8(1)	385.2(1)	0.956	0.0541	1
U_2AuSi_3	AlB_2	414.5(3)	398.9(2)	0.962	0.0593	6
UAuSi	LiBaSi	419.5(2)	397.2(2)	0.947	0.0605	this work
UAu_2	AlB_2	475.6(2)	311.0(1)	0.654	0.0609	this work
UAu_2	AlB_2	475.4	310.7	0.654	0.0608	4
UAu_2	AlB_2	475.6	311.0	0.654	0.0609	3
UAu_2	$CeCd_2$	475.6	310.9	0.654	0.0609	5

[a] Standard deviations in the positions of the least significant digits are given in parentheses throughout the paper.

Crystal structures

The crystal structure of UAu_2 is confirmed The lattice parameters [$a=475\,6(2)$ pm, $c=311\,0(1)$ pm] are in excellent agreement with the previous data (Table 1)[3,5] The powder patterns of our UAu_2 samples always showed the AlB_2 structure, independent of the annealing processes, in agreement with the work of Palenzona and Cirafici[3] and Tran and Troc[4] However, Dommann and Hulliger[5] reported a $CeCd_2$-type structure for UAu_2 In this structure type, the gold atoms are not situated on the mirror plane at $z=0\,5$, they are shifted to $z\approx0\,45$, resulting in slightly puckered layers

We have calculated theoretical powder patterns with LAZY-PULVERIX[11] in order to check the two possibilities For the $CeCd_2$-type structure two reflections at $2\theta=63\,94°$ and $76\,74°$ should occur with intensities of 6 5 and 4 8 (scaled at an intensity of 100 for the strongest reflection), respectively Both reflections are calculated with intensities of 0 1 for the AlB_2-type structure None of our samples showed these reflections on the Guinier powder patterns However, for comparison, the 001 and 111 reflections with calculated intensities of 4 8 and 7 5, respectively, are clearly visible on the patterns We therefore conclude that UAu_2 adopts the AlB_2-type structure (Fig 1) and there is no evidence for a puckering of the hexagonal gold nets in UAu_2 Positional parameters and interatomic distances are listed in Table 2

For UAuSi we find a different symmetry than that reported previously[10] All our powder patterns (melted samples and those annealed at 650 and 800 °C) show hexagonal symmetry and an intensity distribution resembling the AlB_2-type structure This result was also reproduced for other samples The refined lattice parameters of the sample annealed at 800 °C are $a=419\,5(2)$ pm and $c=397\,2(2)$ pm However, Tran and Troc[10] reported the TiNiSi-type structure for UAuSi (arc-melted sample annealed at 650 °C for 7 days) with the orthorhombic lattice constants $a=418\,1$ pm, $b=798\,2$ pm and $c=724\,1$ pm These values correspond to the doubled orthohexagonal cell of AlB_2 $a_{ortho}=a_{hex}$, $b_{ortho}=2c_{hex}$ and $c_{ortho}=a_{hex}\sqrt{3}$ A reinvestigation of the previously reported[10] powder data indeed showed that UAuSi has the small AlB_2-like hexagonal cell (Fig 2)

In order to establish whether or not the gold and silicon atoms are ordered within the hexagonal network, we have performed powder diffraction measurements on the arc-melted and the annealed samples The order can be detected directly from the sub-cell intensities, since the ordered structure has the *translationengleiche*[18] subgroup $P\bar{6}m2$ The crystallographic relationship for such order–disorder transitions has already

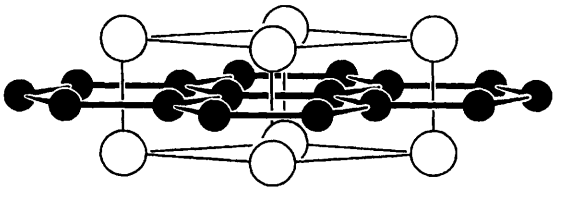

Fig. 1 Crystal structure of UAu_2 ○, uranium, ●, gold The two-dimensional gold network is outlined

Table 2 Positional parameters and interatomic distances (in pm) of UAu_2

atom		*P6/mmm*	*x*	*y*	*z*
U		1a	0	0	0
Au		2d	1/3	2/3	1/2
U	12	Au 315 6(1)	Au	3 Au	274 6(1)
	2	U 311 0(1)		2 Au	311 0(1)
	6	U 475 6(2)		6 U	315 6(1)

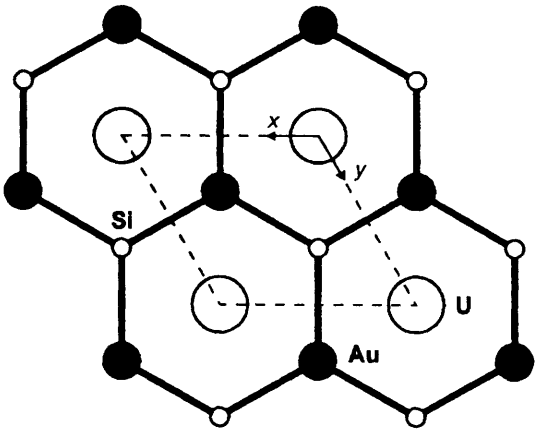

Fig. 2 Crystal structure of UAuSi projected along the *z* direction All atoms are situated on mirror planes at $z=0$(U) and $z=1/2$ (Au, Si) connected by thin and thick lines, respectively

been discussed in detail for isotypic ThAuSi[13] For the sample annealed at 800 °C, we clearly established the ordered LiBaSi-type structure[19,20] The intensities resulting from the Rietveld powder refinements are given in Table 3 Positional parameters and interatomic distances are listed in Table 4

In contrast, the collected powder diagrams of the arc-melted sample and the sample annealed at 650 °C show two very similar hexagonal cells Several reflections already showed some splitting on the Guinier powder patterns From this result we assumed that only a certain part of the samples is ordered The Rietveld powder refinements (assuming two phases) showed about 70% LiBaSi-type and about 30% AlB_2-type structures in the sample annealed at 650 °C The refined lattice parameters (powder diffraction data) were $a=419\,25(3)$ pm, $c=398\,14(2)$ pm, $V=0\,0606$ nm^3 for the LiBaSi portion and $a=420\,79(5)$ pm, $c=395\,98(5)$ pm, $V=0\,0607$ nm^3 for the AlB_2 portion As could be expected, the cell volume of the disordered AlB_2 part is slightly larger than that of LiBaSi The order within the LiBaSi-type structure expresses itself by the smaller lattice parameter *a* and a larger lattice parameter *c* We conclude from this refinement, that (i) the annealing temperature of 650 °C was slightly too low to achieve complete order, or (ii) the annealing time of 2 weeks was too short for this temperature

Lattice constants

The lattice parameters and the cell volumes of the compounds in the pseudobinary system USi_2–UAu_2 are given in Table 1 As can be seen easily from these data, the *a* and *c* parameters increase slightly, when some silicon atoms in β-USi_2 are replaced by the much larger (metallic radii 131 9 pm for Si and 144 2 pm for Au, both for coordination number, CN, 12)[21] gold atoms The increase of both is small up to UAuSi and then the situation is different While *a* rises dramatically up to UAu_2, *c* behaves in the opposite manner

Crystal chemistry

A part of the pseudobinary system USi_2-UAu_2 has been investigated by X-ray powder diffraction All patterns show hexagonal symmetry The border phases β-USi_2[1] and UAu_2[3,5] adopt the AlB_2-type structure For UAuSi we have determined an order between the gold and silicon atoms They form a hexagonal BN-like network The previously reported intermetallic U_2AuSi_3 did not show any order between the Au and Si atoms, however, ordered structures for 2 1 3 silicides were recently reported for the compounds Ln_2RhSi_3,[22,23] Ln_2PdSi_3[24] and U_2RuSi_3[8]

The silicon atoms in β-USi_2 are thus substitutable by gold

Table 3 X-Ray powder data of UAuSi (sample annealed at 800 °C); the observed (I_o) and calculated (I_c) intensities for both refinements (disordered AlB_2-type and LiBaSi-type) are listed together with the corresponding residuals $R_B(I)$[a]

			AlB_2 type			LiBaSi type		
hkl	$2\theta_{obs}$/degrees	d_{calc}/Å	I_o	I_c	I_o-I_c	I_o	I_c	I_o-I_c
100	24.45	3.6334	22350	16314	6036	24324	24783	459
101	33.35	2.6823	100000	100567	567	100000	98485	1515
110	43.06	2.0977	35665	36527	862	33121	32943	178
002	45.55	1.9883	9600	9929	329	9081	9086	5
111	49.03	1.8554	689	716	27	145	146	1
200	50.14	1.8167	2567	2676	109	3615	3641	26
102	52.38	1.7442	4633	4693	60	4846	4821	25
201	55.54	1.6524	17274	17515	241	17760	17691	69
112	64.49	1.4431	15893	14683	1210	15605	15138	467
210	68.21	1.3733	342	316	26	276	264	12
202	70.08	1.3412	2128	2016	112	2170	2086	84
003	71.03	1.3256	125	119	6	22	22	0
211	72.77	1.2981	12497	11776	721	13461	12918	543
103	76.39	1.2453	5307	4853	454	5670	5373	297
300	78.96	1.2111	3419	3092	327	3706	3491	215
301	83.31	1.1586	658	598	60	119	112	7
212	85.92	1.1300	2590	2372	218	1776	1663	113
113	86.82	1.1206	619	570	49	116	108	8
203	91.97	1.0708	2572	2404	168	2792	2691	101
220	94.48	1.0489	1594	1503	91	1917	1847	70
302	96.24	1.0343	2929	2797	132	3545	3464	81
221	98.81	1.0142	474	468	6	95	93	2
310	99.67	1.0077	667	660	7	510	503	7
				$R_B(I)=0.049$			$R_B(I)=0.018$	

[a] The final residuals for the refinement with the ordered LiBaSi structure are $R_{wp}=0.1025$, $R_E=0.0652$ and $\chi^2=2.4714$.

Table 4 Positional parameters and interatomic distances (in pm, calculated from the Guinier data) for UAuSi

atom	$P\bar{6}m2$		x	y		z	B/Å^2
U	1a		0	0		0	2.2(7)
Au	1f		2/3	1/3		1/2	3.6(16)
Si	1d		1/3	2/3		1/2	1.7(35)
U:	6 Au	313.2(2)	Au: 3 Si	242.2(1)	Si:	3 Au	242.2(1)
	6 Si	313.2(2)	6 U	313.2(2)		6 U	313.2(2)
	2 U	397.2(2)					
	6 U	419.5(2)					

atoms up to the other border phase, UAu_2. This substitution reveals not only a drastic change in the lattice parameters as discussed above, but also a change in the coordination spheres, resulting in distinct differences in chemical bonding. A comparison of the interatomic distances in β-USi_2, U_2AuSi_3, UAuSi and UAu_2 is given in Table 5.

In β-USi_2 the U–U distances of 385.2 and 402.8 pm are similar. This is totally different when all the silicon atoms are substituted by gold atoms. The U–U bond lengths in UAu_2 amount to 311.0 and 475.6 pm, respectively. While both U–U distances in β-USi_2 may not be considered as direct U–U interactions, the small U–U contact of 311.0 pm in UAu_2 is certainly strongly bonding. Similar short U–U distances have also be observed in the intermetallics U_2Mn_3Ge,[25] U_2Ti,[26–28] U_3Si[29] and UHg_2.[30] They are in the same range as in α-U (average U–U bond length of 313.7 pm).[31] The coordination of the uranium atoms in β-USi_2 consists of 12 silicon atoms. Owing to the short U–U contacts, this coordination number increases to 14 in UAu_2; 12 Au and 2 U.

Table 5 Comparison of the interatomic distances (in pm) in the structures of β-USi_2, U_2AuSi_3, UAuSi and UAu_2

compound	U–U	U–Au/Si	Au/Si–Au/Si
β-USi_2	385.2 402.8	302.0	232.6
U_2AuSi_3	398.9 414.5	311.5	239.3
UAuSi	397.2 419.5	313.2	242.2
UAu_2	311.0 475.6	315.6	274.6

The U–Au/Si distances increase from 302.0 pm (β-USi_2) to 311.5 pm in U_2AuSi_3 and then increase only slightly to 315.6 pm in UAu_2. The slightly larger U–Au distance in UAu_2 also reflects the larger coordination number of 14.

The interatomic distances within the hexagonal network increase from 232.6 (β-USi_2) to 242.2 pm (UAuSi) and then increase markedly to 274.6 pm in UAu_2. The increase of only 9.6 pm (the difference of the metallic radii amounts to 12.3 pm[21]) from β-USi_2 to UAuSi reflects the strong bonding between the gold and silicon atoms. The Au–Si distance of 242.2 pm is about 12% smaller than the sum of the metallic radii. It is even smaller than the Au–Si bond lengths of 249, 249, 252 and 246 pm in ScAuSi (ScAuSi-type), YAuSi (LiGaGe-type), LuAuSi (ScAuSi-type)[32] and ThAuSi (LiBaSi-type, isotypic with UAuSi),[13] respectively. In the Au_6 rings of UAu_2, the Au–Au distances of 274.6 pm are about 5% smaller than the Au–Au bond lengths of 288 pm in gold metal.[31] The coordination number for the atoms in the hexagonal network increases from CN 9 in β-USi_2 (6 U + 3 Si) to CN 11 in UAu_2 (6 U + 3 Au + 2 Au).

Physical properties

UAuSi. In order to derive the influence of atomic ordering of Au and Si atoms on the physical properties of UAuSi, the temperature dependence of the magnetic susceptibility and electrical resistivity was studied on three samples of UAuSi: (i) as-quenched, (ii) annealed at 650 °C and (iii) annealed at 800 °C.

We have measured $\chi(T)$ in magnetic fields up to 0.6 T employing both the ZFC (zero magnetic field cooling) and FC (field cooling) conditions. It appears that these three samples show almost identical temperature dependencies of the magnetic susceptibility, similar to that already reported in ref. 10. In Fig. 3 we present the magnetic data for UAuSi (iii) only.

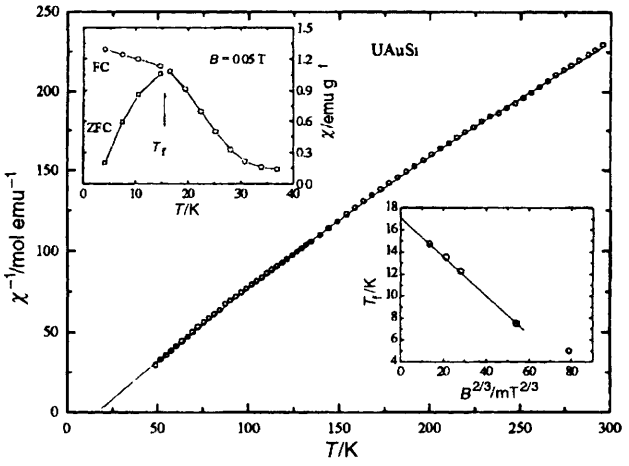

Fig. 3 Temperature dependence of the reciprocal magnetic susceptibility of UAuSi The left-hand inset shows the FC and ZFC susceptibility behaviour at $B=0.05$ T The field dependence of the freezing temperature, T_f, is shown in the right-hand inset

As seen from the inset, the FC susceptibility shows a weak saturation tendency at low temperatures, while the ZFC susceptibility exhibits a maximum at T_f (freezing temperature) Thus, the temperature dependence of the magnetic susceptibility for this compound appears to be strongly dependent on the sample cooling conditions The observed anomaly at T_f may indicate a magnetic phase transition, however, this maximum is broad and its magnitude is too large to be ascribed to a simple antiferromagnetic phase transition Such a maximum might signal a transition into an anisotropic ferromagnet, but the magnetization behaviour of UAuSi (III) taken at various temperatures below 40 K in magnetic fields up to 4 T does not show characteristics of a ferromagnet As seen from Fig 4, the magnetization, $\sigma(B)$, does not show saturation at 4 2 K At the highest obtainable magnetic field of $B=4$ T, only the very

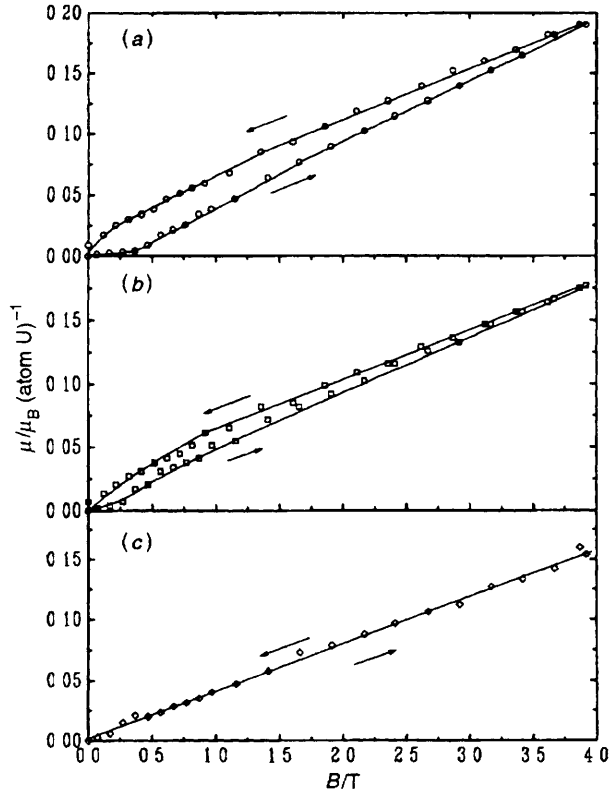

Fig. 4 Magnetization *vs* magnetic flux density of UAuSi at (*a*) 4 2, (*b*) 20 and (*c*) 40 K

small magnetic moment of $\mu=0.19$ μ_B (atom U)$^{-1}$ is observed However, at temperatures between 4 2 and 20 K, a small remanence is present in $\sigma(B)$

As suggested in ref 10, the χ anomaly is thought to originate from spin-glass (SG) behaviour Therefore, we have investigated the irreversibility line from $\chi_{ZFC}(T)$ and $\chi_{FC}(T)$ taken in several magnetic fields Defining the freezing temperature, T_f, as the splitting point of the χ_{ZFC} and χ_{FC} curves, we have determined T_f as a function of the applied magnetic field (see Fig 3 inset) It is clear that T_f follows well the theoretical Almeida and Thouless line (AT line)[33] in the low magnetic field limit, strongly supporting the SG-like behaviour for UAuSi The extrapolated T_f value to $B=0$ is about 17 K This value of T_f is almost the same as that found in our previous electrical resistivity measurements [10] It should be mentioned that the AT straight line was predicted for the case of an Ising-type SG in the infinite-range, random-bond model [33] On the other hand, as shown above, the magnetic properties of UAuSi are found not to depend on the degree of the atomic order and therefore such an interpretation for UAuSi is not quite adequate Also, at present it is difficult to claim that any non-stoichiometry of this compound is a possible reason of the SG-behaviour observed

SG-behaviour is found for numerous uranium- and rare-earth-metal-based intermetallics crystallizing in hexagonal structures, such as $CeCd_2$-type (UCuSi),[34] AlB_2-type (U_2TSi_3),[7] and $Ln(Al,Ga)_2$ [35] For all these hexagonal phases the XY-type mechanism seems to be responsible for the SG-formation Also, the existence of some randomness in the interactions between the U–U or Ln–Ln atoms, since a statistical distribution of the non-magnetic atoms in the unit cell of a given compound can lead to the SG properties This mechanism has been postulated for $CePd_3B_{0.3}$ [36] and $CePtGa_3$ [37]

For all samples of UAuSi, the magnetic susceptibility is reversible above T_f and reaches almost the same values As seen from Fig 3, the $\chi^{-1}(T)$ function shows modified Curie–Weiss behaviour, yielding $\mu_{exp}=3.14$ μ_B (U atom)$^{-1}$, $\Theta=-17.1$ K and $\chi_o=0.3\times10^{-3}$ emu mol^{-1} These values are in agreement with those reported in ref 10

In contrast to the χ(T) behaviour, the temperature dependence of the electrical resistivity changes for different sample preparation methods The electrical resistivity measurements as a function of temperature, $\rho(T)$, for the three samples of UAuSi are given in Fig 5 While the resistivity of the samples which are non-annealed or annealed at 650 °C increases with decreasing temperature in a Kondo-like manner, the resistivity of the sample annealed at 800 °C, *i e* of that showing full

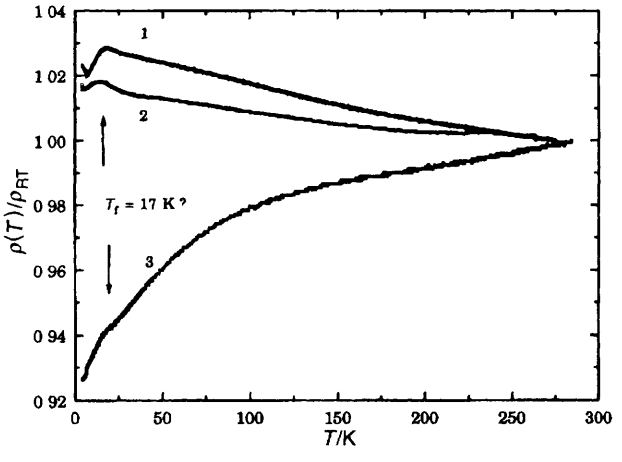

Fig. 5 Temperature dependence of the reduced electrical resistivity for the three different UAuSi samples The spin freezing temperature is indicated by arrows 1, as-cast, 2, annealed at 650 °C, 3, annealed at 800 °C

crystallographic order, decreases distinctly with decreasing temperature (metal-like behaviour). Also important differences occur in the magnitude of ρ. The resistivity of samples (i) and (ii) is about an order of magnitude larger than that of sample (iii). These differences certainly reflect some variation in the degree of the crystallographic order of the Au and Si atoms. Nevertheless, there exists a common feature for all these samples, namely, the ρ anomaly occurring at about 17 K. This temperature should be associated with the T_f value deduced from the extrapolation to $B=0$ T (see Fig. 3). Note that the occurrence of the resistivity maximum is one of the most distinctive features of the metallic-type SG.[38] Thus, this behaviour may be characteristic of samples (i) and (ii).

UAu_2. The low-temperature properties of UAu_2 have already been reported in a number of previous investigations of the U–Au system.[4,39–41] However, serious controversy concerning the magnetic properties observed for this compound still remains. For example, Ott *et al.*[39] were the first group to report Pauli paramagnetism of UAu_2, but they assigned the $CeCd_2$-type structure for their sample. On the other hand, the annealed UAu_2 sample had the hexagonal AlB_2-type structure, and both the magnetic susceptibility and the electrical resistivity pointed to the existence of a weak ferromagnetic component below 25 K.[4] Moreover, Kondo-type behaviour or spin-fluctuation effects have also been considered by Canepa *et al.*[40] or recently by Kontani *et al.*,[41] respectively.

In the present investigation we have used the annealed UAu_2 sample for the measurements. Its magnetic susceptibility *vs* temperature curve is displayed in Fig. 6. Above $T=50$ K the susceptibility behaviour for this sample obeys the Curie–Weiss law yielding $\mu_{exp}=2.98\ \mu_B$ (atom U)$^{-1}$ and $\Theta=-190$ K. These values agree well with those previously reported for a non-annealed sample[40] but they are slightly different from those found for an annealed sample by Kontani *et al.*[41] As illustrated in Fig. 6, the susceptibility of our UAu_2 sample exhibits a pronounced upturn below $T=30$ K. This behaviour, which is a consequence of oxidation, will be analysed in detail in a forthcoming paper.[42]

The temperature dependence of the electrical resistivity for the annealed sample of UAu_2 is displayed in Fig. 7. This curve is similar to that recently reported by Kontani *et al.*[41] $\rho(T)$ shows a pronounced increase in resistivity at low temperatures, and then a broad shoulder followed by saturation in the high-temperature region. This result resembles the $\rho(T)$ behaviour characteristic of materials dominated by spin-fluctuation effects.[43] The temperature derivative of the resistivity, $d\rho(T)/dT$ exhibits a distinct maximum at 18 K. Some tiny anomalies are also observed at 8 and 40 K. They are probably due to impurities and were also observed by Kontani *et al.*[41]

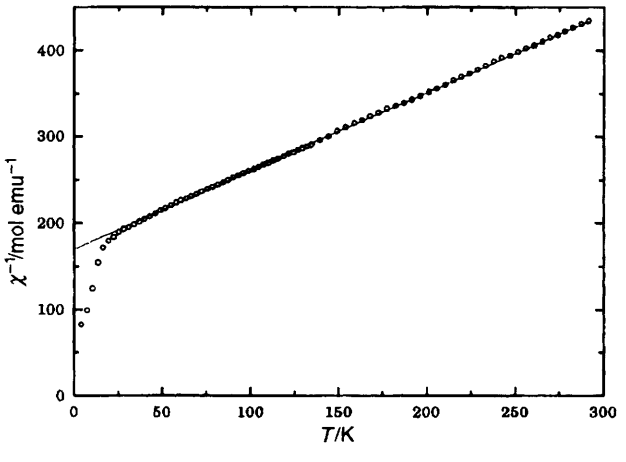

Fig. 6 Temperature dependence of the inverse magnetic susceptibility of UAu_2 (annealed, 800 °C, 2 weeks, $B=0.7$ T)

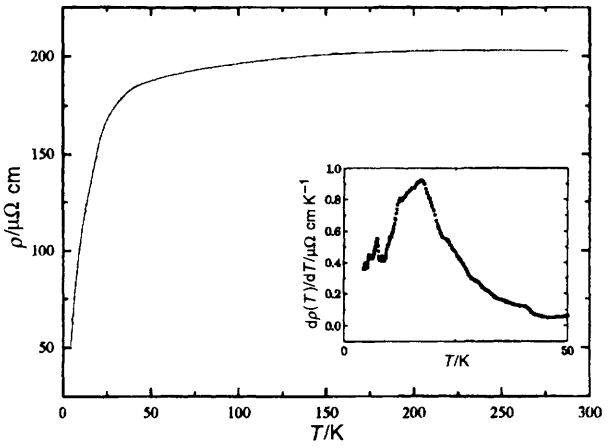

Fig. 7 Temperature dependence of the specific resistivity of UAu_2 (annealed, 800 °C, 2 weeks, $B=0$ T). The inset shows the derivative $d\rho/dT$ *vs.* T below 50 K.

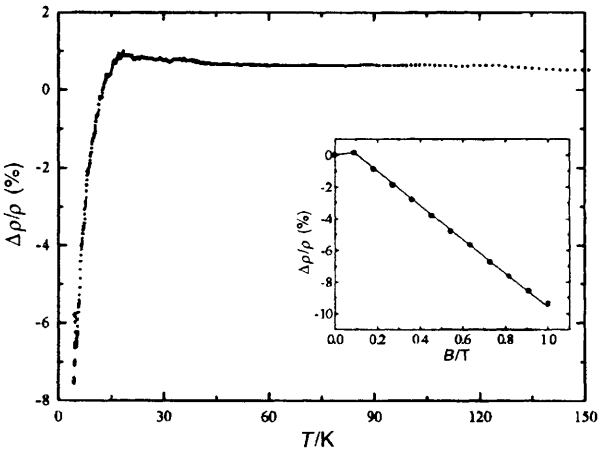

Fig. 8 Temperature dependence of the magnetoresistivity of UAu_2 (annealed, 800 °C, 2 weeks, $B=1$ T). The field dependence of the magnetoresistivity at 4.2 K is given in the inset.

In order to clarify the nature of the anomalies observed for UAu_2 we undertook measurements of the electrical resistivity at $B=1$ T. It is interesting to note that the transition observed at 40 K starts to develop distinctly at $B=1$ T, but no visual change has been observed in the transitions at 8 and 18 K, respectively.

The magnetoresistivity, $\Delta\rho/\rho=[\rho(T,1\text{T})-\rho(T,0)]/\rho(T,0)$, measured as a function of temperature, is displayed in Fig. 8. At 4.2 K, the magnetoresistivity is negative and decreases linearly with increasing applied magnetic field without any tendency to saturation (see Fig. 8 inset). As the temperature is increased, the $\Delta\rho/\rho$ curve increases, starting from a value of -8%, goes through zero at about 15 K, and then reaches a distinct maximum at 18 K. At higher temperatures, this curve remains almost unchanged, showing a positive value. The negative magnetoresistivity observed at low temperatures is in agreement with some ferromagnetic character of the sample.

We thank Professor Dr. W. Jeitschko for his interest and support of this work. We are also indebted to Dr. W. Gerhartz (Degussa AG) for a generous gift of gold metal and to the Fonds der Chemischen Industrie for a stipend to R. P.

References

1 A. Brown and J. J. Norreys, *Nature*, 1959, **183**, 673.
2 K. Remschnig, T. Le Bihan, H. Noël and P. Rogl, *J. Solid State Chem.*, 1992, **97**, 391.
3 A. Palenzona and S. Cirafici, *J. Less-Common Met.*,1988, **143**, 167.

4 V H Tran and R Troc, *20ièmes Journees des Actınıdes*, Abstract P7, Prague, Aprıl 17–20, 1990
5 A Dommann and F Hullıger, *J Less-Common Met* ,1988, **141**, 261
6 R Pottgen and D Kaczorowskı, *J Alloys Comp* , 1993, **201**, 157
7 D Kaczorowskı and H Noel, *J Phys Condens Matter*, 1993, **5**, 9185
8 R Pottgen, P Gravereau, B Darrıet, B Chevalıer, E Hıckey and J Etourneau, *J Mater Chem* , 1994, **4**, 463
9 B Chevalıer, R Pottgen, B Darrıet, P Gravereau and J Etourneau, *J Alloys Comp* , ın press
10 V H Tran and R Troc, *Physıca B*, 1993, **186–188**, 744
11 K Yvon, W Jeıtschko and E Parthe, *J Appl Crystallogr* , 1977, **10**, 73
12 F Izumı, Rıetveld analyses programs RIETAN and PREMOS and specıal applıcatıons, ın *The Rıetveld Method*, ed R A Young, Internatıonal Unıon of Crystallography, Oxford Unıversıty Press, 1993, pp 236–253
13 J H Alberıng, R Pottgen, W Jeıtschko, R-D Hoffmann, B Chevalıer and J Etourneau, *J Alloys Comp* , 1994, **206**, 133
14 U Zachwıeja, *J Alloys Comp* , 1993, **196**, 187
15 U Zachwıeja, *J Alloys Comp* , 1993, **196**, 171
16 U Zachwıeja, *Z Anorg Allg Chem* , 1993, **619**, 1095
17 U Zachwıeja, *J Alloys Comp* , 1994, **206**, 277
18 H Barnıghausen, *Commun Math Chem* , 1980, **9**, 139
19 H Axel, K H Janzon, H Schafer and A Weıss, *Z Naturforsch , Teıl B*, 1968, **23**, 108
20 G Wenskı and A Mewıs, *Z Anorg Allg Chem* , 1986, **535**, 110
21 E Teatum, K Gschneıdner Jr and J Waber, Rep LA-2345, US Department of Commerce, Washıngton, DC, 1960
22 B Chevalıer, P Lejay, J Etourneau and P Hagenmuller, *Solıd State Commun* , 1984, **49**, 753
23 R E Gladyshevskıı, K Cenzual and E Parthe, *J Alloys Comp* 1992, **189**, 221
24 P A Kotsanıdıs, J K Yakınthos and E Gamarı-Seale, *J Magn Magn Mater* , 1990, **87**, 199
25 R Pottgen, B Chevalıer, R-D Hoffmann, W Jeıtschko and J Etourneau, *J Alloys Comp* , to be publıshed
26 M C Udy and F W Boulger, Trans AIME, 1954, **200**, 207
27 A G Knapton, *J Inst Metals, London,* 1955, **83**, 497
28 B W Howlett, *J Nucl Mater* , 1959, **3**, 289
29 G Kımmel, B Sharon and M Rosen, *Acta Crystallogr , Sect B* 1980, **36**, 2386
30 R E Rundle and A S Wılson, *Acta Crystallogr* , 1949, **2**, 148
31 J Donohue, *The Structures of the Elements*, Wıley, New York, 1974
32 M L Fornasını, A Iandellı and M Panı, *J Alloys Comp* 1992, **187**, 243
33 J R L de Almeıda and D J Thouless, *J Phys A* , 1978, **11**, 983
34 V H Tran and R Troc, *J Magn Magn Mater* , 1990, **86**, 231
35 A R Ball, D Gıgnoux, D Schmıtt and F Y Zhang, *J Magn Magn Mater* , 1992, **104&107**, 170
36 S K Dhar, K A Gschneıder Jr , C D Bredl and F Steglıch, *Phys Rev B* , 1989, **39**, 2439
37 J Tang, K A Gschneıder Jr , R Caspary and F Steglıch, *Physıca B*, 1989, **163**, 201
38 P J Ford and J A Mydosh, *Phys Rev B*, 1976, **14**, 2057
39 H R Ott, E Felder, A Schılling, A Dommann and F Hullıger, *Solıd State Commun* , 1989, **71**, 549
40 F Canepa, A Palenzona and R Eggenhoffner, *Physıca B*, 1990, **160**, 297
41 M Kontanı, T Nıshıoka, Y Hamaguchı, H Matsuı, H A Katorı and T Goto, *J Phys Soc Jpn* , 1994, **63**, 3421
42 R Troc *et al* , to be publıshed
43 T Morıya, ın *Spın Fluctuatıons ın Itınerant Electron Magnetısm*, Springer, Berlın, 1985

Paper 5/04446D, *Received 7th July*, 1995